Chinese Chemical Letters 37 (2026) 111041

Contents lists available at ScienceDirect

Chinese Chemical Letters

journal homepage: www.elsevier.com/locate/cclet

NIR-II absorbing aza-BODIPY with the D-A-A' framework for PTT/PDT co-therapy

Xin Zhang[a,1], Ziyue Xi[b,1], Dongxiang Zhang[a], Lu Xu[b,*], Yunsheng Xue[c,*], Xin-Dong Jiang[a,*], Gaowu Qin[a]

[a] Liaoning & Shenyang Key Laboratory of Functional Dye and Pigment, Shenyang University of Chemical Technology, Shenyang 110142, China
[b] School of Pharmacy, Shenyang Pharmaceutical University, Shenyang 110016, China
[c] Jiangsu Key Laboratory of New Drug Research and Clinical Pharmacy, School of Pharmacy, Xuzhou Medical University, Xuzhou 221004, China

ARTICLE INFO

Article history:
Received 5 November 2024
Revised 3 March 2025
Accepted 5 March 2025
Available online 7 March 2025

Keywords:
Aza-BODIPY
NIR-II
D-A-A' framework
PTT/PDT co-therapy
4T1 tumor

ABSTRACT

Classic near-infrared dyes typically enhance their maxima absorption wavelength through the D-A system. Herein, introducing *p*-trifluoromethylphenyl group at 1,7-sites as electron-withdrawing group and julolidine at 3,5-sites as electron-donating group in aza-borondipyrromethene (aza-BODIPY) system, **CF_3-JLD** with the donor-acceptor-acceptor (D-A-A') system was prepared, which absorbs at 952 nm and emits at 1069 nm in dimethyl sulfoxide (DMSO) in the near infrared-II (NIR-II) region. According to the experimental observation and theoretical calculation, the D-A-A' system for enhancing redshift of maxima absorption is found to be more effective than that of donor-acceptor-donor (D-A-D') system. NIR-II absorbing **CF_3-JLD** was type I photodynamic therapy/photothermal therapy (PDT/PTT) co-therapy reagent, with high photothermal conversion efficiency ($\eta = 81\,\%$). Self-assembled nanoparticles (**CF_3-JLD** NPs) can effectively induce 4T1 cell death *in vitro*, and the cellular morphology of tumor was destroyed and the proliferation-related protein was decreased *in vivo* under NIR irradiation by phototherapy. This strategy of the D-A-A' system provides a guideline for developing organic fluorophores with enhanced NIR-II absorption and type I PDT/PTT co-therapy for 4T1 breast tumors.

© 2025 Published by Elsevier B.V. on behalf of Chinese Chemical Society and Institute of Materia Medica, Chinese Academy of Medical Sciences.

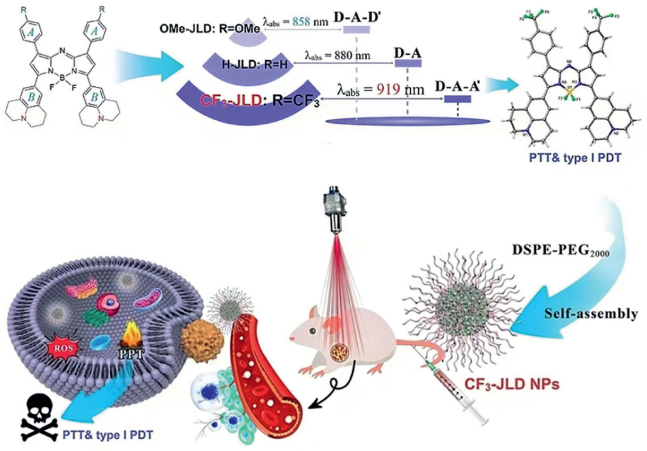
Photofunctional dyes with strong absorption and emission in the second near infrared (NIR) window (NIR-II, 900–1700 nm) show great value in phototherapy and fluorescence imaging [1–6], due to a deep penetration depth for deep-seated tissues, ultra-low photon scattering and diminished autofluorescence in biological tissues, compared to those in the NIR-I region (700–900 nm) [7–13]. Moreover, the extended wavelength could effectively reduce the sensitivity of the tissue to light in photothermal or photodynamic therapy (PTT/PDT) [14–16]. Especially, PTT/PDT co-therapy, in contrast to chemo and gene therapy, allows precise and spatiotemporal destruction of tumor tissue, with no significant damage to normal tissue and negligible drug resistance, and therefore, has attracted increasing interest as an advantageous method for tumor treatment [17–22]. Since PTT/PDT requires light irradiation of dyes to function properly, NIR-II absorbing photofunctional dyes are crucial during this non-invasive treatment [23–25].

In fact, NIR-II absorbing photofunctional dyes, including polymethine dyes, donor–acceptor–donor (D–A–D) dyes, are very scarce [26–29]. However, traditional NIR-II dyes also have flaws such as poor stability originated from large conjugated structures, and difficult modification [30]. Compared with these traditional dyes, aza-borondipyrromethenes (aza-BODIPYs) possess a stable structure, large molar extinction coefficient and tuned wavelength [31,32]. So, the advancements in the development and design strategies of NIR-II aza-BODIPY fluorophores tailored for advanced biological phototheranostics [6].

For a single molecule, NIR-II absorbing aza-BODIPY, most of the design strategies were based on the insertion of the donor group to the parent nucleus of aza-BODIPY as the electron acceptor to construct the D-A type delocalized skeleton. The strong D-A system could efficiently promote spectral bathochromic-shift by reducing the energy gap between highest occupied molecular orbital (HOMO) and lowest unoccupied molecular orbital (LUMO) [33–35]. Julolidine, as an important nitrogen-containing segment, has attracted much attention in recent years due to its electron-rich and highly planar properties [36,37]. The strong electron-donor of julolidine is superimposed with the electron-acceptor of aza-BODIPY

* Corresponding authors.
E-mail addresses: xulu@syphu.edu.cn (L. Xu), ysxue77@xzhmu.edu.cn (Y. Xue), xdjiang@syuct.edu.cn (X.-D. Jiang).
[1] These authors contributed equally to this work.

https://doi.org/10.1016/j.cclet.2025.111041
1001-8417/© 2025 Published by Elsevier B.V. on behalf of Chinese Chemical Society and Institute of Materia Medica, Chinese Academy of Medical Sciences.



Scheme 1. Schematic illustration of energy differences in system categories, preparation of self-assembled **CF_3-JLD** NPs and theranostic mechanisms.

core to produce the super D-A system. This in turn drives a larger intramolecular charge transfer effect (ICT), resulting in remarkably bathochromic shift [38]. Therefore, the combination of julolidine with aza-BODIPY to form the D-A system is a novel design strategy. For instance, Huang *et al.* reported that the NIR-II absorbing aza-BODIPY with the julolidine segment was achieved by modifying the julolidine group at 1,7-sites in the aza-BODIPY system [39]. Our group has been focusing on studies on this design in the aza-BODIPY system [40]. According to the reported literature, the electron-donor groups at 3,5-sites in aza-BODIPY system indeed have a greater impact on the spectral properties than those of 1,7-sites [41,42].

It is worth noting that in the above reports, the D-A-D' system for dye is popularly adopted for reduction of LUMO–HOMO gap energy [43]. However, in julolidine-containing aza-BODIPY system, D-A-A' system for enhancing redshift of maxima absorption is first found to be more effective than that of D-A-D' system (Scheme 1). Through extensive comparison, aza-BODIPY of D-A-A' system was found to have larger absorption wavelength and better spectroscopic properties (Table S1 in Supporting information). Since extending conjugated structure of aza-BODIPY results in instability, we only introduce *p*-trifluoromethylphenyl group at 1,7-sites as electron-withdrawing group and julolidine at 3,5-sites as electron-donating group when involving the core of 1,7,3,5-tetraphenyl aza-BODIPY (λ_{abs} = 640 nm), structuring the D-A-A' system of a novel dye **CF_3-JLD** (λ_{abs} = 956 nm in DMSO) (Scheme 1). The prepared **CF_3-JLD** with *p*-trifluoromethylphenyl group have larger absorption than those replaced by methoxyl group (λ_{abs} = 850 nm) or the hydrogen atom (λ_{abs} = 880 nm) in the corresponding position. On this basis, we further investigated the photothermal and photodynamic properties, and carried out biological cell toxicity with cells and mice. These results showed that the dye-nanoparticles could effectively kill cells and eliminate tumors in mice under light excitation. Therefore, this study provides a strategy for the D-A-A' design of NIR-II absorbing aza-BODIPY as type I PDT/PTT co-therapy reagent.

Utilizing 9-acetyljulolidine generated by Friedel-Crafts acylation, target compound aza-BODIPY **CF_3-JLD** was smoothly prepared by 15.5% total yield (Scheme S1 in Supporting information). Moreover, the structure of **CF_3-JLD** was undoubtedly confirmed by a single crystal X-ray analysis (Fig. 1a). Based on crystallographic structure, the angles of N5-B1-F1 (111.3°), N3-B1-F2 (110.9°), F1-B1-F2 (110.8°) and N3-B1-N5 (107.39°), are near to the ideal value of 109.5°, indicating the boron atom in the center is a slightly distorted sp^3 configuration (Fig. 1a). Additionally, according to the

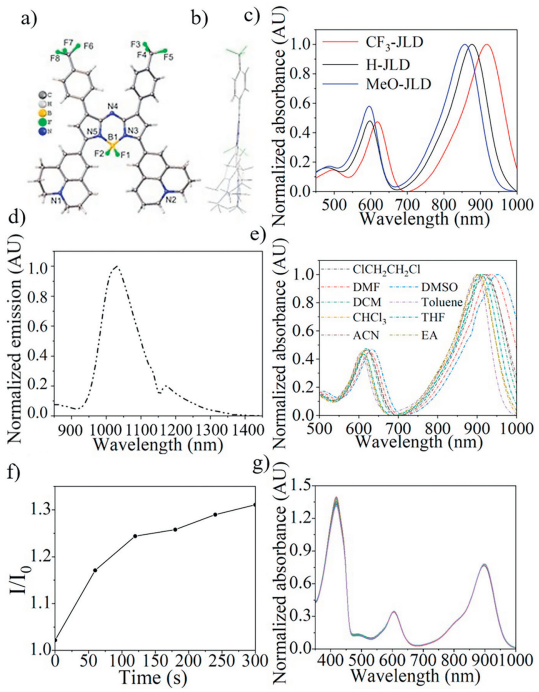


Fig. 1. (a) Oak Ridge thermal ellipsoid plot (ORTEP) views of **CF_3-JLD** (CCDC: 2380901). (b) Side views of the molecular structure. Selected angles (°): N5-B1-F1, 111.3(2); N3-B1-F2, 110.9(2); F1-B1-F2, 110.8(2); N3-B1-N5, 107.39(19). (c) Normalized absorption spectra of aza-BODIPY with *p*-trifluoromethyl phenyl, phenyl and p-methoxyphenyl group at 1,7-sites in CH_2Cl_2. (d) Normalized emission spectrum of **CF_3-JLD** in CH_2Cl_2. λ_{ex} = 808 nm; the slit is 5 nm. (e) Absorption spectra of **CF_3-JLD** in solvents. (f) ROS generation of **CF_3-JLD** (5 μmol/L) in THF under continuous 808 nm laser (0.3 W/cm^2) irradiation for 5 min using DCFH (10 μmol/L) as an indicator. (g) $^1O_2$ generation efficiency of **CF_3-JLD** with time when DPBF is the indicator.

side view, including the boron atom, the nucleus of **CF_3-JLD** is coplanar (Fig. 1b).

To gain insight into the specific impact of the substituents on spectral performance, the strictly compared molecules (**H-JLD** and **OMe-JLD**) were synthesized (Scheme 1 and Table S2 in Supporting information). Compared with tetraphenyl aza-BODIPY (λ_{abs} = 640 nm in CH_2Cl_2) [42], a dramatically bathochromic shift of 279 nm was observed in **CF_3-JLD** (λ_{abs} = 919 nm), owing to the introduction of the strong electron-donating and electron-withdrawing groups. Unexpectedly, the maximum absorption of **OMe-JLD** in the D-A-D' system was found to hypochromatically shift to 858 nm in CH_2Cl_2, while the maximum absorption of **CF_3-JLD** bearing the D-A-A' system bathochromically shifted be 919 nm yet, comparing to that of the parent dye **H-JLD** (λ_{abs} = 880 nm) (Fig. 1c). So, to understand theoretically the photophysical and electronic properties of aza-BODIPYs **H-JLD**, **CF_3-JLD** and **OMe-JLD**, we carried out theoretical calculations. Table S3 (Supporting information) gives the calculated maxima absorption wavelength, oscillator strength and the assignment of main absorption peaks, using the PCM-TD-B3LYP(GD3)/6–311+G(d) method. As can be seen from Table S3, the calculated $\lambda_{max,abs}$ results are in good agreement with the experimental values. The two main absorption peaks correspond to the transition of S_1 and S_2 excited states respectively, for all the three compounds. The S_1 state is ascribed to exciting an electron from HOMO to LUMO, while the S_2 state is from HOMO-1 to LUMO. As shown in Fig. S1 (Supporting information), HOMO and HOMO-1 are mostly distributed on the aza-BODIPY core and the phenyl ring *B*, while the LUMO are mainly located on the BODIPY core and the phenyl ring *A* (Scheme 1), thus these two states are of partial charge-transfer character, indicating that reduction of the energy gap HOMO-LUMO prefers D-A-A' system in aza-BODIPYs.

Therefore, the lower energy gap (ΔE_1 and ΔE_2) in **CF_3-JLD** implies redshift of the $\lambda_{max,abs}$ compared to that of **H-JLD**, while blueshift of the $\lambda_{max,abs}$ for **OMe-JLD** (Fig. S1). These results are in line with the experimental observation.

And, **CF_3-JLD** has high molar extinction coefficients ($\varepsilon = 187{,}000\,L\ mol^{-1}\ cm^{-1}$) and broad full width at half maximum (FWHM = 123 nm) in CH_2Cl_2, comparing to that (116 nm) of **H-JLD** or **OMe-JLD** (Table S2), just indicating that non-radiative transitions lead to more energy loss during the de-excitation process of **CF_3-JLD**. Indeed, the rotational barrier for the $-CF_3$ group of **CF_3-JLD** is about 0.12 kcal/mol (Fig. S2 in Supporting information), indicating that the rotation of $-CF_3$ group in solution is very easy. This causes more system energy (such as heat) to be released through the non-radiative way. Additionally, the maximum emission of **CF_3-JLD** is 1029 nm in CH_2Cl_2 within NIR-II region (Fig. 1d), even reaching 1069 nm in DMSO (Fig. S3 in Supporting information), but its fluorescence quantum yield is so low to be 0.01. Furthermore, the solvent effect of **CF_3-JLD** is also investigated (Fig. 1e). It was found that when the solvent changed from toluene to DMSO, the maxima absorption is from 898 nm to 952 nm respectively, due to the effect of solvent polarity. Meanwhile, we explored the effect of **CF_3-JLD** on the aggregation mode, and the absorption spectra variation of **CF_3-JLD** in the mixed solution of tetrahydrofuran (THF) and H_2O was recorded (Fig. S4 in Supporting information). It was found that when the mixture ratio of THF and H_2O was 1:1, the maxima absorption redshifted to 936 nm, and the corresponding absorption maximum in THF solution was 908 nm (Fig. 1e).

Next, using 2′,7′-dichlorodihydrofluorescein (DCFH) as an indicator, the overall reactive oxygen species (ROS) generation in THF solution was monitored by continuously irradiating **CF_3-JLD** with 808 nm laser (0.3 W/cm^2) for 5 min. As shown in Fig. 1f, with increase of laser irradiation time, the generation of ROS continues to increase. The results showed that the fluorescence intensity was enhanced by about 1.3 times under illumination, indicating that **CF_3-JLD** has an ability of ROS production under light trigger. To further identify the type of ROS, utilizing 1,3-diphenylisobenzofuran (DPBF) as the singlet oxygen ($^1O_2$) indicator, the exposure time was regulated to track the $^1O_2$ generation efficiency (Fig. 1g). Fig. 1g exhibited that the $^1O_2$ generation efficiency of **CF_3-JLD** was very low. Subsequently, using DHR123 as an indicator, **CF_3-JLD** was irradiated with 808 nm (0.3 W/cm^2) continuously for 5 min to monitor the production of ROS in DMSO solution. As shown in Fig. S5a in Supporting information, the ROS generation efficiency of **CF_3-JLD** increases with the increase of laser irradiation time. The results show that the fluorescence intensity of **CF_3-JLD** is increased by about 1.2 times under laser irradiation, which proves that **CF_3-JLD** has ROS generation ability under light-triggered conditions. This indicated that superoxide radical ($O_2^{\bullet-}$) was generated and this is a photosensitizer (PS) of type I PDT [44].

To simulate the biological environment and enhance the compatibility of **CF_3-JLD** in biological system, we employed 1,2-distearoyl-*sn*–glycero-3-phosphoethanolamine-*N*-[methoxy(polyethylene glycol)–2000] (DSPE-PEG_{2000}) to prepare self-assembled nanoparticles (**CF_3-JLD** NPs). Based on transmission electron microscopy (TEM) photograph (Fig. 2a), the spherical morphology of the nanoparticles was clearly observed, their sizes were not beyond 150 nm, and the zeta potential was about 108.2 mV (Fig. S6 in Supporting information), indicating that **CF_3-JLD** NPs are stable. Dynamic light scattering (DLS) of **CF_3-JLD** NPs exhibited a suitable hydrodynamic diameter (50–120 nm) in Fig. 2b, and the average hydrodynamic diameter and the polydispersity index (PDI) of **CF_3-JLD** NPs were about 77.3 nm and 0.33, respectively. After placed in aqueous solution for two weeks, no precipitate was observed and the particle size did not change significantly, suggesting that **CF_3-JLD** NPs are stable in aqueous solution (inner

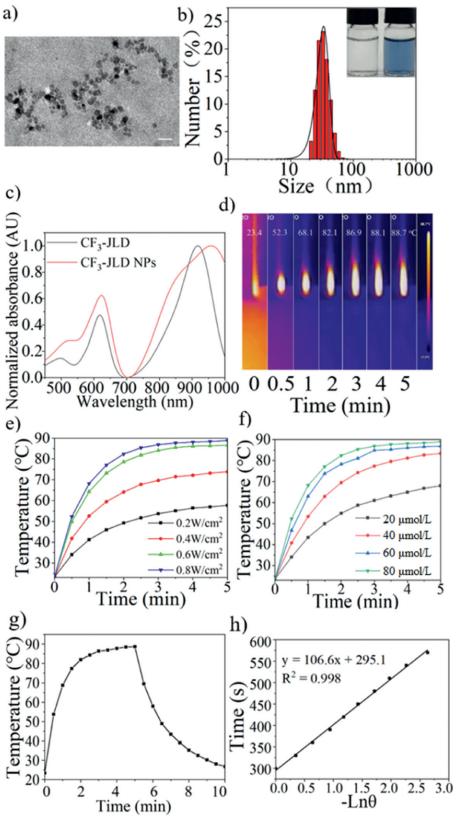


Fig. 2. (a) Morphology of **CF_3-JLD** NPs under transmission electron microscopy. Scale bar: 100 nm. (b) Size distribution of **CF_3-JLD** NPs in aqueous solution. Inner panel for the photo of pure water (left) and **CF_3-JLD** NPs in water (right). (c) Absorption of **CF_3-JLD** (black curve) in CH_2Cl_2 and **CF_3-JLD** NPs (red curve) in aqueous solution. (d) Photos of the photothermal effect (23.4–88.7 °C). (e) Photothermal effect of **CF_3-JLD** NPs under different power conditions. (f) Photothermal effect of **CF_3-JLD** NPs under different concentration conditions. (g) Temperature changes in the heating–cooling phase. (h) Cooling time *versus* the negative natural logarithm of driving force temperature.

panel of Fig. 2b). Compared to that ($\lambda_{abs} = 919$ nm) of **CF_3-JLD** in CH_2Cl_2, the maximum absorption value ($\lambda_{abs} = 956$ nm) of **CF_3-JLD** NPs in aqueous solution shifted by 37 nm and produced a wider absorption peak belt (700–1300 nm) in NIR-II region (Fig. 2c), due to the aggregation effect. Additionally, based on DHR123 as an indicator, **CF_3-JLD** NPs had also ROS generation ability under light-triggered conditions (Fig. S5b in Supporting information), suggesting that superoxide radical ($O_2^{\bullet-}$) was produced.

Next, the photothermal properties of **CF_3-JLD** NPs have been detailedly studied (Fig. 2d and Figs. S7–S9 in Supporting information). Using an 808 nm laser as a light source, a NIR camera is employed to record the temperature change of 80 μmol/L **CF_3-JLD** NPs in aqueous solution during this process (Fig. 2d). When irradiating for 30 s, the temperature rapidly increased from 23.4 °C to 55.6 °C. After the irradiation for 5 min, the temperature rose to 88.7 °C, with temperature difference of 65.3 °C (Fig. 2d). Then, we chose the concentration of 80 μmol/L **CF_3-JLD** NPs to discuss the influence on temperature by utilizing different powers of 808 nm laser (0.2–0.8 W/cm^2) (Fig. 2e). Based on Fig. 2e, the temperatures are also proportional to the laser power. Then, different concentrations of **CF_3-JLD** NPs were prepared to investigate the influence of the concentration on photothermal effect. As shown in Fig. 2f, the temperatures showed a positive correlation with the increase of the concentration of **CF_3-JLD** NPs. Subsequently, five rounds of temperatures monitoring during the cycle of 5 min light radiation and 5 min cooling were conducted (Fig. S10). The findings demon-

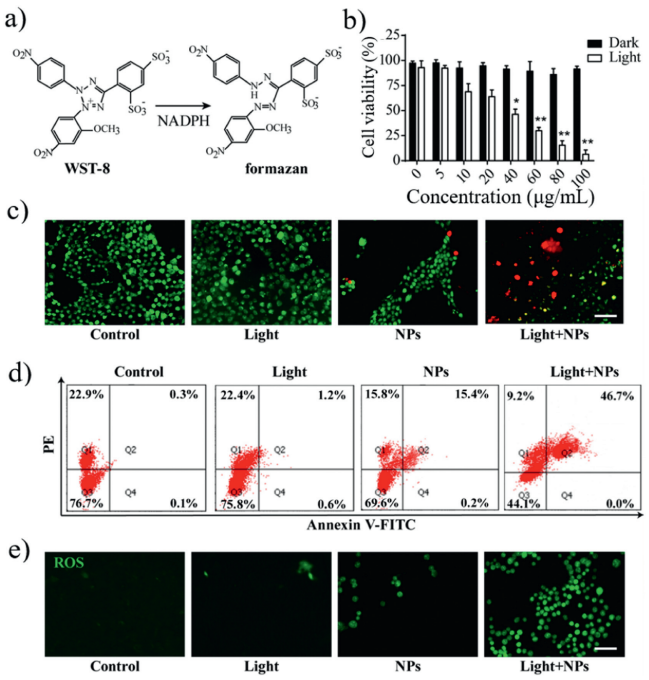


Fig. 3. Photothermal effect of **CF_3-JLD** NPs under 808 nm laser irradiation on the proliferation ability of 4T1 cell. (a, b) Schematic of CCK-8 methods and cell viability analyzed by CCK-8 assay in 4T1 cell lines under different concentrations with 808 nm laser irradiation. NADPH, nicotinamide adenine dinucleotide phosphate. (c) Fluorescence images of calcine AM and PI co-stained 4T1 cells. (d) Apoptosis levels of 4T1 cells by flow cytometry assay. (e) Confocal laser scanning microscope (CLSM) images of intracellular ROS level from four groups of 4T1 cells. Scale bar: 20 μm. Data are presented as mean ± SD ($n = 3$). $^{*}P < 0.05$, $^{**}P < 0.01$ *vs.* control group (20 μg/mL CF3-JLD NPs).

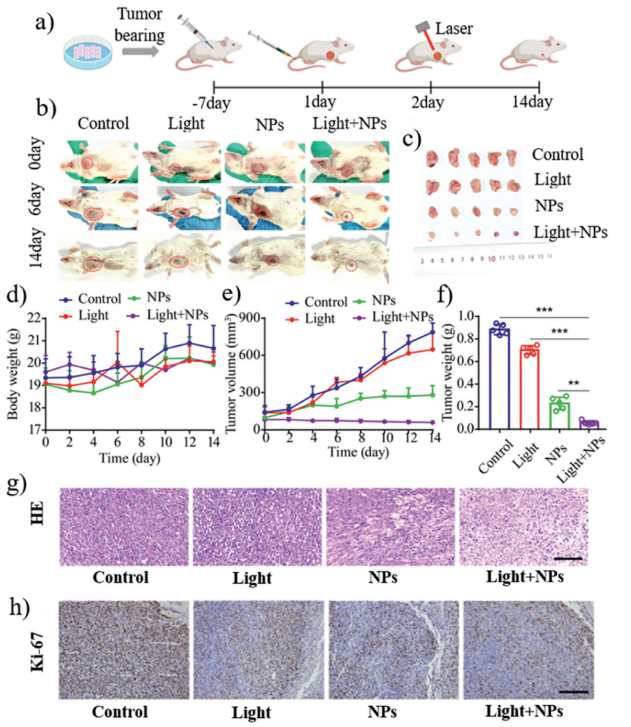


Fig. 4. Anti-tumor activity of **CF_3-JLD** NPs for 4T1 tumor-bearing mice *in vivo*. (a) Schematic treatment schedule for treatment *in vivo*. (b) Images for tumor growth condition for different days. (c) Tumor growth curves. (d) Body weight changes and (e) dissected tumor volume of bright light images of different groups. (f) Tumor weights of mice with treatments. (g) HE stained images of the intracranial tumor area after different treatments (200×). (h) Immunohistochemical Ki-67 stained images of the intracranial tumor from four groups (200×). Scale bar: 100 μm. Data are presented as mean ± SD ($n = 5$). $^{**}P < 0.01$, $^{***}P < 0.001$.

strated that the solution could be heated from room temperature 23.4 °C to 88.7 °C after heating for 5 min, and the temperature almost reduced to room temperature during the same time span of natural cooling. The maximum temperature variation was almost negligible, indicating that **CF_3-JLD** NPs had good photostability. Furthermore, to investigate the photothermal conversion efficiency, the associated time constant obtained by mapping the cooling time and driving force temperature was brought into the reported formula for calculating the photothermal conversion efficiency. The photothermal conversion efficiency of **CF_3-JLD** NPs was very high and calculated to be 81 % (Figs. 2g and h), comparing to those of the reported literatures [32,45,46].

Next, the phototoxicity of **CF_3-JLD** NPs in 4T1 cells was analyzed by cell counting kit-8 (CCK-8) kit. The mechanism of CCK-8 to detect the cytotoxicity was displayed as Fig. 3a, based on fluorescence differences caused by ring opening. When the laser was off, the cell viability was exhibited high values (>85 %) as a dose-dependent phenomenon (Fig. 3b). The cell viability was also 88.86 % at the highest concentration, indicating that the great biocompatibility of **CF_3-JLD** NPs without irradiation. When exposed to NIR (0.3 W/cm^2, 808 nm) for 3 min, the cell viability was decreased obviously with the higher concentrations of **CF_3-JLD** NPs. The survival cancer cells were only occupied with 8.2 % at the highest concentration. The results showed that the NIR-triggering photothermal effect by **CF_3-JLD** NPs could kill 4T1 cells effectively (Fig. 3b). For further confirm the phototoxicity and phototherapeutic capacity of **CF_3-JLD** NPs, the calcein AM (green) and propidium iodide (PI, red) dyes were employed to stained live/dead cells. In detailed, the green fluorescence was labeled live cells and red fluorescence was labeled dead cells in Fig. 3c. In control and light groups, there were no injury cells due to the absent of **CF_3-JLD** NPs, according to the whole green area. For **CF_3-JLD** NPs group without irradiation, a large area of green and limited red area for 4T1 cells were observed, indicating that **CF_3-JLD** NPs could not display a photothermal effect without laser stimulation. For light+**CF_3-JLD** NPs group, obvious red area and enhanced fluorescence intensity were observed, suggesting the improved toxicity was induced by the combined NIR and **CF_3-JLD** NPs. Moreover, flow cytometry assay was conducted to quantify the apoptosis level of 4T1 cells (Fig. 3d). The apoptosis cells and necroptosis cells were stained with Annexin-V and PI. The early and late apoptosis of 4T1 cells were distributed at fourth and second quadrants, respectively [47]. The percentage of apoptosis cells (in Q2) were 0.3 %, 1.2 %, 15.4 % and 46.7 % for control, light, **CF_3-JLD** NPs and light+**CF_3-JLD** NPs groups, respectively (Fig. 3d). The higher apoptosis rate of light+**CF_3-JLD** NPs group after the treatment with 0.3 W/cm^2 from an 808 nm NIR laser for 3 min suggested the efficient phototherapeutic capacity of **CF_3-JLD** NPs. The accumulation of ROS might induce cell apoptosis [48].

Therefore, DCFH-DA was selected as a ROS probe to assess the ROS production ability of **CF_3-JLD** NPs with irradiation. As shown in Fig. 3e, compared to other groups, remarkable green florescence intensity was observed in light+**CF_3-JLD** NPs group. The results suggested that ROS was accumulated in 4T1 cells with the coexistence of the **CF_3-JLD** NPs and NIR irradiation. Combined with the above results, **CF_3-JLD** NPs can effectively induce 4T1 cell death under NIR irradiation by phototherapy.

Inspiring by the excellent phototherapy effect of Light+**CF_3-JLD** NPs, we further explore the *in vivo* antitumor effect of **CF_3-JLD** NPs in 4T1 breast tumor-bearing mice (Fig. 4a). All of the animal experiment procedures herein were permitted by the Animal Ethics Committee of Sciences of Shenyang Pharmaceutical University. The tumor-bearing mice were randomly divided into four

groups: control, light, **CF_3-JLD** NPs and light+**CF_3-JLD** NPs. The initial tumor volumes of four groups were all about 100 mm^3. After treatment of 6–14 days, the tumor of light+**CF_3-JLD** NPs group was minimal, compared to other groups as shown in Fig. 4b. Moreover, the control and light groups had no inhibitory effect on tumor growth for 14 days and the tumor inhibition effect of **CF_3-JLD** NPs group was limited. As shown in Figs. 4c–f, the volumes of tumor increased rapidly for control, light and **CF_3-JLD** NPs group, suggesting that single laser irradiation and **CF_3-JLD** NPs alone both had no suppression capacity on tumor growth. In contrast, the tumor volumes of light+**CF_3-JLD** NPs group were obvious inhibition for 14 days and the final dissected tumor was in small size and weight (56.37 mm^3, 45.2 mg). Additionally, no distinct weight loss of the body in different groups was observed, indicating the stable biosafety of **CF_3-JLD** NPs. As expected, the light+**CF_3-JLD** NPs group exhibited significantly enhanced tumor growth inhibitory rate than single **CF_3-JLD** NPs or light groups, which attributed to NIR-triggering phototherapy effect of **CF_3-JLD** NPs for better antitumor efficiency. Simultaneously, hematoxylin-eosin staining (HE) and immunohistochemistry of Ki-67 images further confirmed the large injury area of tumor tissues and limited proliferated ability of light+ **CF_3-JLD** NPs group. In detailed, it was observed that the cellular morphology of tumor was destroyed (Fig. 4g) for light+**CF_3-JLD** NPs group and the proliferation-related protein was decreased obviously (Fig. 4h). Meanwhile, it was no obvious pathological changes appeared in HE staining of major organs (heart, liver, spleen and kidney), demonstrating that the superior biocompatibility of **CF_3-JLD** NPs (Fig. S11 in Supporting information).

Utilizing 9-acetyljulolidine generated by Friedel-Crafts acylation, target compound aza-BODIPY **CF_3-JLD** was smoothly prepared by 15.5 % total yield. The structure of **CF_3-JLD** was undoubtedly confirmed by a single crystal X-ray analysis, and the boron atom in the center is a slightly distorted sp^3 configuration. Compared with tetraphenyl aza-BODIPY ($\lambda_{abs} = 640$ nm in CH_2Cl_2), a dramatically bathochromic shift of 279 nm was observed in **CF_3-JLD** ($\lambda_{abs} = 919$ nm). The maximum absorption of **OMe-JLD** in the D-A-D' system was found to hypochromatically shift to be 858 nm in CH_2Cl_2, while the maximum absorption of **CF_3-JLD** bearing the D-A-A' system bathochromically shifted be 919 nm yet, comparing to that of the parent dye **H-JLD** ($\lambda_{abs} = 880$ nm). HOMO and HOMO-1 are mostly distributed on the aza-BODIPY core and the phenyl ring *B*, while the LUMO are mainly located on the BODIPY core and the phenyl ring *A*, thus these two states are of partial charge-transfer character, indicating that reduction of the energy gap HOMO-LUMO prefers D-A-A' system in aza-BODIPYs. Based on the ROS generation, superoxide radical ($O_2^{\bullet -}$) was generated and this is a PS of type I PDT. When irradiating the solution of self-assembled nanoparticles (**CF_3-JLD** NPs) for 5 min, the temperature rapidly increased from 23.4 °C to 88.7 °C, with temperature difference of 65.3 °C. The photothermal conversion efficiency of **CF_3-JLD** NPs was very high and calculated to be 81 %. **CF_3-JLD** NPs can effectively induce 4T1 cell death *in vitro*, and the cellular morphology of tumor was destroyed and the proliferation-related protein was decreased *in vivo* under NIR irradiation by phototherapy. The findings of this study suggest that our work offers a robust design strategy of the D-A-A' system for the development of aza-BODIPY phototherapy agents in the NIR-II region.

Declaration of competing interest

The authors declare that they have no known competing financial interests or personal relationships that could have appeared to influence the work reported in this paper.

CRediT authorship contribution statement

Xin Zhang: Methodology, Formal analysis, Data curation. **Ziyue Xi:** Resources, Methodology, Conceptualization. **Dongxiang Zhang:** Writing – original draft. **Lu Xu:** Writing – review & editing. **Yunsheng Xue:** Writing – original draft, Software. **Xin-Dong Jiang:** Writing – review & editing, Supervision. **Gaowu Qin:** Writing – review & editing.

Acknowledgments

This work was supported by the National Natural Science Foundation of China (Nos. 22078201, U1908202), Liaoning & Shenyang Key Laboratory of Functional Dye and Pigment (Nos. 2021JH13/10200018, 21–104–0–23, LJKZ0453), Department of Science & Technology of Liaoning Province (No. 2022JH2/20200056). We also thank Prof. Yohsuke Yamamoto (Hiroshima University) for his help.

Supplementary materials

Supplementary material associated with this article can be found, in the online version, at doi:10.1016/j.cclet.2025.111041.

References

[1] L. Yang, L. Jiang, F. Xu, et al., Sens. Actuators B: Chem. 379 (2023) 133251.
[2] R.X. Wang, Y. Ou, Y. Chen, et al., J. Am. Chem. Soc. 146 (2024) 11669–11678.
[3] L. He, L.H. He, S. Xu, et al., Angew. Chem. Int. Ed. 61 (2022) e202211409.
[4] K. Wei, Y. Wu, X. Zheng, et al., Angew. Chem. Int. Ed. 63 (2024) e202404395.
[5] D. Ma, H. Bian, M. Gu, et al., Coord. Chem. Rev. 505 (2024) 215677.
[6] L. Zhang, C. Yan, Y. Zhang, et al., Chem. Commun. 59 (2023) 8388–8391.
[7] C. Yan, Z. Zhu, Y. Yao, et al., Acc. Mater. Res. 5 (2024) 64–75.
[8] W. Zhang, Z. Hu, C. Fang, et al., Ann. Transl. Med. 9 (2021) 171.
[9] J. Cao, B. Zhu, K. Zheng, et al., Front. Bioeng. Biotechnol. 7 (2020) 487.
[10] W. Zhu, Sci. China Chem. 59 (2016) 203–204.
[11] M.E. Shirbhate, S. Kwon, A. Song, et al., J. Am. Chem. Soc. 142 (2020) 4975–4979.
[12] S. Cheung, D.F. O'Shea, Nat. Commun. 8 (2017) 1885.
[13] L. Bao, J. Bian, Y. Yan, et al., Biomed. Pharmacother. 88 (2017) 1220–1226.
[14] T. Pu, Y. Liu, Y. Pei, et al., ACS Appl. Mater. Interfaces 15 (2023) 32226–32239.
[15] X. Ren, S. Han, Y. Li, et al., Anal. Chem. 96 (2024) 8689–8695.
[16] G. Wang, Q. Qiao, N. Xu, et al., Sens. Actuators B: Chem. 417 (2024) 136155.
[17] X. Guo, L. Li, W. Jia, et al., ACS Appl. Mater. Interfaces 16 (2023) 19926–19936.
[18] J. Lin, B. Xing, D. Jin, Adv. Opt. Mater. 11 (2023) 2300802.
[19] J. Hou, J. Jie, X. Wei, et al., J. Nanobiotechnol. 22 (2024) 449.
[20] Y. Tao, C. Yan, Y. Wu, et al., Adv. Funct. Mater. 33 (2023) 2303240.
[21] R. Chang, Q. Zou, L. Zhao, et al., Adv. Mater. 34 (2022) e2200139.
[22] D. Wu, J.C. Ryu, Y.W. Chung, et al., Anal. Chem. 89 (2017) 10924–10931.
[23] Y. Hu, J.F. Honek, Q.B. Lu, et al., J. Biophot. 12 (2019) e201900129.
[24] S. Li, R. Chang, L. Zhao, et al., Nat. Commun. 14 (2023) 5227.
[25] Y. Wang, L. Chang, H. Gao, et al., Eur. J. Med. Chem. 272 (2024) 116508.
[26] B. Li, M. Zhao, F. Zhang, ACS Mater. Lett. 2 (2020) 905–917.
[27] D. Yao, Y. Wang, R. Zou, et al., ACS Appl. Mater. Interfaces 12 (2020) 4276–4284.
[28] Y. Yang, Y. Xie, F. Zhang, Adv. Drug Deliv. Rev. 193 (2023) 114697.
[29] M. Chen, Z. Zhang, R. Lin, et al., Chem. Sci. 15 (2024) 6777–6788.
[30] Z. She, R. Li, S. Wu, et al., Adv. Health. Mater. 13 (2024) e2400791.
[31] Y. Xu, S. Wang, Z. Chen, et al., J. Nanobiotechnol. 19 (2021) 37.
[32] X. Hu, Z. Fang, C. Zhu, et al., Adv. Funct. Mater. 34 (2024) 2401325.
[33] L. Bai, P. Sun, Y. Liu, et al., Chem. Commun. 55 (2019) 10920–10923.
[34] H. Chen, G. Cai, A. Guo, et al., Macromolecules 52 (2019) 6149–6159.
[35] P. Li, Y. Jia, S. Zhang, et al., Inorg. Chem. 61 (2022) 3951–3958.
[36] Z. Fang, J. Zhang, Z. Shi, et al., Adv. Mater. 35 (2023) e2301901.
[37] J. Varejão, E. Varejão, S. Fernandes, Eur. J. Org. Chem. 2019 (2019) 4273–4310.
[38] M. Kaur, A. Janaagal, I. Gupta, et al., Coord. Chem. Rev. 498 (2024) 215428.
[39] Z. Shi, H. Bai, J. Wu, et al., Research 6 (2023) 0169.
[40] L. Cao, Z. Cui, D. Zhang, et al., ACS Mater. Lett. 6 (2024) 4765–4773.
[41] R. Li, J. Ren, D. Zhang, et al., Mater Today Bio 16 (2022) 100446.
[42] A. Gorman, J. Killoran, C. O'Shea, et al., J. Am. Chem. Soc. 126 (2004) 10619–10631.
[43] D. Mo, T. Tong, Q. Zhang, et al., New J. Chem. 48 (2024) 7590–7598.
[44] Y. Zhu, F. Wu, B. Zheng, et al., Nano Lett. 24 (2024) 8287–8295.
[45] Y. Zhu, J. Liu, M. Lv, et al., Chin. Chem. Lett. 35 (2024) 109446.
[46] L. Cao, Y. Li, D. Zhang, et al., Chin. Chem. Lett. 35 (2024) 109735.
[47] L. Zhou, W. Feng, L. Chen, et al., Nano Today 46 (2022) 101623.
[48] C. Glorieux, S. Liu, P. Huang, et al., Nat. Rev. Drug Discov. 23 (2024) 583–606.